
Monograph:
Edwards, J.B. and Mohd Noor, S.B. (1996) The Simulation Testing of Analytically-Derived, Steady-State and Transfer-Function Models for CSTC Binary Distillation Columns. Research Report. ACSE Research Report 630 . Department of Automatic Control and Systems Engineering

---

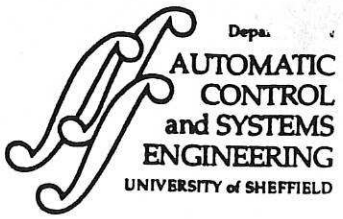

The Simulation Testing of Analytically-Derived, Steady-State and Transfer-Function Models for CSTC Binary Distillation Columns

by;

J. B. Edwards and S. B. Mohd Noor

Process Control and Automation Research Group
Department of Automatic Control and System Engineering
The University of Sheffield
Mappin Street
Sheffield S1 3JD
United Kingdom

ACSE Research Report No: 630

July 1996

The Simulation Testing of Analytically-Derived, Steady-State and Transfer-Function Models for CSTC Binary Distillation Columns

J. B. Edwards and S. B. Mohd Noor

Abstract

Parametric steady-state and transfer-functions models, analytically-derived for separation occurring within a packed CSTC distillation column reported in ACSE RR573, 1995 are here validated by comprehensive time domain simulation. Both large-signal steady-state and small-signal dynamic responses are found to be in complete accord with the analytical predictions under both open- and linear, closed-loop control conditions. Differences in large signal behaviour are demonstrated and are explained in terms of the non-linear reversing gain characteristic of the process here derived. The work is undertaken and reported as essential preliminaries to using the models for future behavioural prediction, in particular under the On Line Riccati Control strategy of Banks[2].

1. Introduction

This report is the third in a series on analytical modelling, control and behavioural prediction of binary distillation columns and chemical reactors. The first report[1] is ACSE RR573, April 95 which presents the analytically derived steady-state and transfer function models in parametric from for columns of the packed type, both distributed (tubular) and approximate stirred-tank (CSTC) versions.

The present report uses exhaustive simulation to validate the CSTC version in both open- and closed-loop situations as a prerequisite for further behavioural prediction and, in particular, before attempting the application of the On-Line Riccati Control technique[2] of Banks. That will be reported in the fourth research report[3], ACSE RR631, 1996, now in preparation. The Banks method has been applied and reported[4] already in ACSE RR576, Dec. 1995, to an idealised, first-order, isothermal CSTR reactor model and subsequently by Rowlands[5] to a second-order, adiabatic CSTR with manipulable cooling and varying temperature effects. These process models are simpler, even compared to even the CSTC reactor model, but indicated significant potential improvements possible in the process control area from utilisation of the On-Line Riccati Control strategy compared to PID. The more involved column models, whilst presenting a more significant challenge in applying the method, offer scope for greater potential improvements in performance as a result of the greater scope offered by their increased state dimension.

The Banks' method, being model based, it is clearly essential that the adequacy of column models, such as the one presented here, are understood as fully as possible. Hence the present report.

The report tests the correctness of the steady state large signal prediction of the analytic CSTC models of RR573 and goes on to compare small signal step responses of the simulated and derived transfer function models. Large signal behaviour is also investigated and the source of significant differences from small signal responses is explained in terms of a large signal steady state characteristic derived here in appendix 1. Section 2 concentrates on steady state and open loop dynamic response whilst Section 3 examines the validity of proportional closed loop stability criteria developed in RR573. As well as the local stability criteria, interesting large signal behaviour is also examined. Throughout the project, a wide range of plant parameter space has been investigated and models validated therefore. Widely spaced typical results are presented here. Conclusions are drawn in Section 4.

2. Testing the CSTC Separation and Gain Formulae

2.1 Formulae to be Tested

ACSE Research Report 573 (Edwards and Mohd Noor : April 1995)[1] developed analytically the following formulae for the steady state gain g_o between small (strictly infinitesimal) changes, δ, in output product separation, S, and total fractional circulating flow $(v+l)/V$, where changes v and l in vapour and reflux rate are kept equal (i.e. $v=l$). The formula is

$$g_o = \frac{\delta}{2\ v/V} = \frac{\alpha\varepsilon}{(\alpha+1)}\left[\frac{\varepsilon L^2 - 4\alpha L - \varepsilon}{\{(3\alpha-1)L+\alpha+1\}^2}\right] \qquad (1)$$

where V denotes quiescent vapour rate $\overline{V}_r$ in the rectifier section of the column, L the normalised length of the rectifier, i.e. :

$$L = \frac{L'k}{V} \qquad (2)$$

where L' is the actual length and k the evaporation rate p.u. length p.u. deviation from equilibrium and α (α^{-1}) is the slope of the equilibrium curve in the rectifying (stripping) section. Parameter ε is given by :

$$\varepsilon = \alpha - 1 \qquad (3)$$

The model is derived for balanced quiescent column operation i.e.

for $\overline{V}_r = \overline{L}_s$ (4)

and $\overline{L}_r = \overline{V}_s$ (5)

where $\overline{L}$ and $\overline{V}$ denote quiescent liquid and vapour molar flow within the column, suffixes r and s distinguishing rectifier and stripping sections. From eqns. (4) and (5), it follows that :

$$\overline{D} = \overline{W} = F \tag{6}$$

where $\overline{D}$ and $\overline{W}$ denote the molar flow rate of top and bottom product respectively under quiescent conditions and F denotes the constant flow rate of vapour feed rate into the column (assumed also equal to the flow of liquid in the feed mixture). The condition :

$$\overline{V}_r = \alpha \overline{V}_s \quad (\text{and hence } \overline{L}_r = \alpha \overline{L}_s) \tag{7}$$

thus making $V \left(= \overline{V}_r\right) = \dfrac{\alpha F}{\varepsilon}$ (8)

and $\overline{V}_s = \dfrac{F}{\varepsilon}$ (9)

is also assumed, being the condition required by tubular columns for even quiescent loading throughout the two sections of the column. These flow conditions were shown in RR573 to produce a quiescent separation given by :

$$S = \frac{\varepsilon}{(\alpha+1)}\left[\frac{(3\alpha+1)L+\alpha-1}{(3\alpha-1)L+\alpha+1}\right] \tag{10}$$

2.2 Simulation Details

The simulation used SIMULINK representation of the bilinear process equations* set out in RR573 i.e. for the column and feed sections :

$$\dot{S} + \frac{V_s(S+\alpha S_e) - \varepsilon V_s + F\{S - \varepsilon/(\alpha+1)\}}{kL'} = S_e - S = -\dot{S}_e - \frac{\alpha V_s\{S_e - S_e(1)\}}{kL'} \tag{11}$$

* Eqns (11) and (12) here are identical to eqns. (132) and (136) in RR573 but with the mistyped sign of ε in eqn. (136) here corrected in (12). The same sign error appeared in source eqn. (32) of which (136) is a restatement purely typographical. The error does not propagate in RR573.

and, for the end vessels :

$$\frac{\alpha H'}{T_n}\dot{S}_e(1) = (V_s + F)\{S - \alpha S_e(1) + \varepsilon\} \tag{12}$$

S denotes the real output separation between top vapour and bottom liquid compositions. S_e is fictitious and denotes its value if the column operated in thermodynamic equilibrium. $S_e(1)$ is also fictitious and denotes the separation that would exist between vapour in equilibrium with the accumulator liquid and liquid in equilibrium with reboiler vapour. $\frac{H'}{VT_n}$ is the normalised time constant, T, of the end-vessels. The derivatives of the three state variables S, S_e and $S_e(1)$ may be extracted to give the non-linear state equations :

$$\dot{S} = -S(A + B\,V_s) + S_e(1 - C\,V_s) + D\,V_s + E\,F \tag{13}$$

$$\dot{S}_e = S - S_e(1 + C\,V_s) + C\,V_s\,S_e(1) \tag{14}$$

$$\dot{S}_e(1) = G\,S\,(V_s + F) - H\,S_e(1)(V_s + F) + J\,(V_s + F) \tag{15}$$

where constants A to J are given (in terms of LV, rather than kL', using eqn. (2)) by :

$$A = 1 + \frac{\varepsilon}{\alpha L} \tag{16}$$

$$B = \frac{1}{L\,V} \tag{17}$$

$$C = \alpha\,B \tag{18}$$

$$D = \varepsilon\,B \tag{19}$$

$$E = \frac{\varepsilon}{L\,V\,(\alpha + 1)} \tag{20}$$

$$G = \frac{1}{\alpha\,V\,T} \tag{21}$$

$$H = \alpha\,G \tag{22}$$

$$J = \varepsilon\,G \tag{23}$$

Fig. 1 is the SIMULINK block diagram representing eqns (13) to (15), constants A to J having been calculated from input parameters α, L, F and T by a merged algebraic routine implementing eqns. (8) and (16) through (23). Process input V_s is the control input to the process and is subjected to various step signals initially for open-loop response validation. Subsequently V_s is to be derived from control equations.

2.3 Steady-State Testing

The quiescent steady state separation formula (10) is first validated by setting input V_s to the constant $\frac{V}{\alpha}$ (i.e. to $\frac{F}{\varepsilon}$)[#] as required to meet our prespecified quiescent operating condition. The process was run to steady state from preset initial conditions (usually zero). The experiment was repeated and values of S recorded for a variety of values for parameters α and L and the values of S achieved in steady-state were found to accord almost identically with those predicted by analytical formula (10). Fig. 2 shows the analytical curve of S versus L for α=2 and 5 and $0 < L < 40$ with points generated by the simulation superimposed. Experimental and predicted numerical values agree to within ± 0.0001 with SIMULINK operating at 16-digit precision. It is concluded therefore that eqn. (10) is reliable for the steady-state prediction of separation S under symmetrical operating conditions (4), (5) and (6) and special loading condition (7).

2.4 Checking the Small-Signal Gain

Having allowed the process to reach steady-state, gain tests were made by applying step perturbations to manipulable flow rate $V_s(t)$ in Fig. 1 and observing the change δ in separation for various L, α combinations, in order to check the small-signal gain formula (1), against the observed ratio $\frac{\delta}{(2\nu/V)}$. Fig. 3 for α=2, L=20 (case (a) in RR573) is typical and shows responses for ν = 1, 5, 10, 20 and 35 % of rectifier quiescent rate V. (Since $V = \overline{V}_r = \alpha\overline{V}_s$, in this case $V = 2\overline{V}_s$ so the changes ν amount to 2, 10, 20, 40 and 70 % of $\overline{V}_s$). The ratio $\frac{\delta}{(2\nu/V)}$ clearly falls as ν is increased as might be expected and indeed δ itself reaches a maximum for ν=0.35V, above which δ falls as illustrated by Fig. 4. At ν=0.85V, there is zero steady-state response and δ becomes negative for even larger

[#] Although the facility exists, no variation of F has been attempted in this series of experiments since response to variable feed has not been an object of ACSE research hitherto and no analytical predictions have been made for this experiment. As regards composition responses to changes in V_s (and L_r), all that is important is the ratio : $\frac{V_s}{\alpha}$ (and $\frac{L_r}{F}$) as analysis shows and as tests have verified. Apart from such verification, therefore, F was set arbitrarily at unity throughout the tests reported here.

v. Figs. 5 and 6 show the responses for case (d) (α=5, L=15), again indicating a maximum attainable separation.

However, for the smaller changes in v, the g_o formula gives a good approximation to the observed ratio $\frac{\delta}{(2v/V)}$ as Figs. 9 and 10 show for the two tests cases α=2, L=20 and α=5, L=15 (cases (a) and (d) in RR573). The curves are clearly asymptotic to the predicted g_o values for small v/V as expected. The reduction in apparent gain for the larger v-perturbations is an inevitable effect of the large-signal behaviour of the process, which imposes a limit on the separation achievable by adjustment of V_s at constant F and given α, as proved in Section 2.5 following.

It is worth noting in passing that, for moderate values of v, the transient step responses of Figs. 3 and 4 show non-minimum phase characteristics as predicted in the linearised system analysis of RR573. This question will be addressed in Section 2.6.

2.5 Large Signal Separation versus V_s Relationship

Equation (10) relating steady-state separation S to L {and hence to V ($=\overline{V}_r$) via relation (2)} is derived for the special loading equation (7) $\overline{V}_r = \alpha\overline{V}_s$. The eqn. (10) does not permit exploration of relationship S versus V_s at constant feed rate F since eqn. (7) implies eqn. (9) i.e. $F = \overline{V}_s\varepsilon$ and hence a constant V_s/F ratio. As shown in Appendix 1 (to this report), if the constraint eqn. (7) is lifted, we obtain the more general steady-state solution :

$$S = \frac{\varepsilon}{\alpha+1}\left[\frac{kL'\{2V_s(\alpha+1)+F\}+\alpha V_s F}{kL'(2\alpha V_s+F)+\alpha V_s F+2\alpha V_s^2}\right] \qquad (24)$$

Formula (10) is obtainable from general case (24) merely by setting $F=V_s\varepsilon$, $V=\alpha V_s$ and normalised length L=kL'/V in accordance with eqn. (2). Because the numerator of (24) is linear and the denominator is quadratic in V_s, the resulting curve of S versus V_s shows a maximum S occurring at :

$$V_s\Big|_{S=S_{max}} = \frac{kL'}{\alpha\{\alpha F+2kL'(\alpha+1)\}}\left[\sqrt{2\alpha F\{\alpha F+kL'(\alpha+1)\}}-\alpha F\right] \qquad (25)$$

Curves of S versus V_s by eqn. (24) are graphed in Figs. 7 and 8 for α=2, L=20 and for α=5, L=15 (i.e. cases (a) and (d) of RR573 respectively) with points obtained from the SIMULINK simulation superimposed for verification. The maximum values of S are indeed found to occur at values of V_s given by eqn. (25). These large-signal results explain the large perturbation responses of Figs. 3 and 4 and, in particular, why there exists a maximum attainable deviation δ despite increasing v beyond a limit, set by eqn. (25). As

an illustration, for case (a), α=2, L=20, setting F=1.0 so that V=2.0, $\overline{V}_F = {}^{2.0}/_{2.0} = 1.0$, so that setting kL' = VL = 40 in eqn. (25) gives V_s=1.66 @ $S=S_{max}$ so that the size of perturbation v needed for change δ in S to be maximum is 1.66-1.0 = 66% i.e. close to the near 70% (35% of V) found in simulation to give maximum δ. (See Figs. 3 and 4).

Finally it is worth noting that the formula (1) for g_o should be derivable by analytic determination of $\frac{\partial S}{\partial V_s}\frac{V}{2}$ from general steady-state separation eqn. (24). Such a derivation awaits a subsequent report but numerical checks here do confirm their agreement at the quiescent points $\overline{V}_s = \frac{F}{\varepsilon}$.

2.6 Open-Loop Dynamic Characteristics

In RR573, 1995 Edwards and Mohd Noor predicted a non-minimum-phase transfer-function for the separation dynamic response over a wide range of plant parameter space. In particular the transfer-function for the special case of zero end vessel capacitance (i.e. for T=0) was found to be :

$$\frac{\delta V}{2v} = g_1(s) = \frac{\alpha\varepsilon}{(\alpha+1)}\left[\frac{\varepsilon L^2 - 4\alpha L - \varepsilon - sL\{\varepsilon+(\alpha+1)L\}}{\{\alpha+1+(3\alpha-1)\}\{\alpha+1+(3\alpha-1)L+2\alpha(L+1)Ls+\alpha L^2 s^2\}}\right] \quad (26)$$

[Note that s here denotes Laplace variable wrt normalised time τ ($=\frac{t}{T_n}$) where base time $T_n = \frac{H}{k}$ where H is the molar capacitance p.u length of the vapour or liquid compartments within the rectifier or stripping section. Variable p was used instead of s in RR573 but the use of these symbols is interchanged here for reasons on consistency with other authors in the area of spatial process modelling]. Equation (26) is only second-order because T=0 in that special case. In general the transfer function is third-order and its analytical expression more complicated. However, its asymptotic behaviour was derived to be as follows :

$$\lim_{|s|\to 0} g_1(s) = \frac{g_o}{1+T_o s} \quad (27)$$

and

$$\lim_{|s|\to \infty} g_1(s) = \frac{-g_\infty}{1+T_\infty s} \quad (28)$$

where steady state gain g_o is given by eqn. (1) (already verified),

$$T_o = \frac{2\alpha L(L+1)+T(L-1)}{(3\alpha-1)L+\alpha+1} + \frac{L\{\varepsilon+(\alpha+1)L\}}{\varepsilon L^2-4\alpha L-\varepsilon} \tag{29}$$

$$g_\infty = \frac{\varepsilon\{\varepsilon+(\alpha+1)L\}^2}{(\alpha+1)\{\alpha+1+(3\alpha-1)L\}\{\varepsilon+(3\alpha+1)L^2\}} \tag{30}$$

and $$T_\infty = \frac{L\{L(\alpha+1)+\varepsilon\}}{\{L^2(3\alpha+1)+\varepsilon\}} \tag{31}$$

For the majority of practical cases, parameters g_o, g_∞, T_o and T_∞ are positive thus yielding non-minimum phase behaviour closely approximated by the second-order transfer function :

$$g_A(s) = \frac{g_o(1-T_1 s)}{1+(T_2+T_3)\,s+T_2T_3\,s^2} \tag{32}$$

where, for the same asymptotic behaviour, RR573 showed that :

$$T_2+T_3 = \frac{g_o(T_o-T_\infty)}{g_o+g_\infty} \tag{33}$$

$$T_1 = \frac{g_oT_\infty+g_\infty T_o}{g_o+g_\infty} \tag{34}$$

and $$T_2T_3 = \frac{g_oT_\infty}{g_\infty}\left[\frac{g_oT_\infty+g_\infty T_o}{g_o+g_\infty}\right] \tag{35}$$

Figs. 9 and 10 compare the step-response of $g_A(s)$ with those obtained from non-linear SIMULINK simulation for α=2, L=20 (case(a)) and α=5, L=15 (case(d)) respectively for end-vessel time constant T=1.0. Step changes $2\nu/V$ = 1.0% and 10.0% are applied in both cases. The responses clearly compare well in the initial stages. Towards steady-state, the smaller input step clearly produces a much closer agreement with the linearised model as would be expected in view of the existence of the soft maximum limits on achievable separation discussed previously and illustrated in Figs. 7 and 8.

2.7 The Effect of End-Vessel Capacitance

Figs. 11(A) and (B) and 12(A) and (B) show that the effect of increasing the normalised end-vessel time constant from 1, to 10 and 50 for cases (a) and (d) respectively, Figs. 11(B) and 12(B) being zoomed versions of the initial response of cases (a) and (d)

respectively. Results from both asymptotic and non-linear process simulations are shown, the latter for small input steps $2v/V = 1.0\%$.

As expected, T has comparatively little effect on the initial response, since the parameter is absent from the high frequency asymptotic model parameters g_∞ and T_∞ - see eqns. (30) and (31). As T is increased, it does slow down the approach to steady-state as can be seen in both cases and as expected from its linear influence of the low-frequency asymptotic time constant, T_0 - see eqn. (29). As this predicts, $\partial T_0/\partial T = (L-1)/\{(3\alpha-1)L+\alpha+1\}$ [=0.184 for case (a) and 0.065 for case (d)] the influence of T on the later stages of the response is more powerful in case (a) than in case (d). The effect of T is not precisely the same on the later stages of the responses of the asymptotic and non-linear processes as inspection of Figs. 11 and 12(A) shows. The differences, however, are largely the result of the slight inequality of the steady states attained by the linear and non-linear models rather than being the result of dynamic mismatch.

3. Closed-Loop Tests

The simulation results presented in the previous section give confidence in the applicability of

(a) the open-loop analytical predictions of RR573 in general and

(b) the open-loop validity of the second-order asymptotic model of eqn. (32) and its associated parametric formulae (29) through (35).

The precise large-signal equations and open-loop transfer-function formula derived in RR573 have been simulation-tested very comprehensively as the foregoing sections of this report have illustrated. The predicted small perturbation behaviour, both transient and steady-state, has been validated under open-loop conditions for small inputs $2v/V=1.0\%$, but the effect of a soft maximum limit on separation (derived analytically here) has been shown to limit the applicability of the small signal model somewhat. Closed-loop experiments may prove more exacting than the open-loop tests since :

(a) the closed-loop predictions are based on the 2nd-order, asymptotic model which must, necessarily deviate from the third-order process model over the mid-frequency range, and

(b) the large transient inputs generated by closed-loop action may drive the process into regions of state space far-removed from the quiescent point around which the linear models (3rd-order and 2nd-order, asymptotic) are derived.

3.1 Checking for Critical Stability

In RR573, based on the second-order, non-minimum-phase asymptotic model $g_A(s)$, defined by eqn. (32) in the present report, it was predicted that the open-loop gain of the process for critical closed-loop stability (under proportional control) is given by :

$$K_c g_o = \frac{g_o(T_o - T_\infty)}{g_o T_\infty + g_\infty T_o} \qquad (36)$$

where K_c is the critical value of controller gain K, and model parameters g_o, g_∞, T_o and T_∞ are related to plant parameters L, α and T by eqns. (29) through (35).

The validity of the prediction has been checked using the simulation of Section 2.2 and Fig. 1, to which is coupled a controller of the form

$$V_s = V_{sref} + \left(\frac{KV}{2}\right)(S_{ref} - S) \qquad (37)$$

where separation and vapour flow references S_{ref} and V_{sref} are steady-state consistent, i.e., for specified parameters L and α, S_{ref} is set according to eqn. (10), viz. :

$$S_{ref} = \frac{\varepsilon}{(\alpha+1)}\left[\frac{(3\alpha+1)L+\alpha-1}{(3\alpha-1)L+\alpha+1}\right] \qquad (38)$$

and V_{sref} and V according to the quiescent operating conditions of eqns. (8) and (9), viz.;

$$V_{sref} = F/\varepsilon \qquad (39)$$

and

$$V = \alpha V_{sref} = \alpha F / \varepsilon \qquad (40)$$

The appearance of the parameter (V/2) as a multiplier of K in control eqn. (37) arises from the fact that the process transfer function g(s) is defined as $\frac{\delta}{(2v/V)}$, (eqn. (1)) so that, for consistency, controller gain K is defined as :

$$K = \frac{2(V_{sref} - V)}{V(S - S_{sref})} \qquad (41)$$

Control eqn. (37) is clearly a manipulated restatement of (41). Its absolute value being unimportant, the value of F was retained set at unity throughout the tests. The simulation was arranged to switch in the desired value of gain K from a zero initial setting at an adjustable time from process initiation. This allowed the controller performance to be examined for both large and small initial deviations from the target steady state specified by S_{ref} and V_{sref}, i.e., if desired, the process could be run up towards steady state on exact, open-loop control, using the closed-loop control of gain K for the final approach phase.

The value of critical gain K_c predicted by eqn. (36) was verified for a range of parameters L and α by running the process close to steady state on open loop control and then

switching in the closed loop controller with values of K set around the predicted K_c value. Fig. 13 is a typical result for case (a) (α=2, L=20, T=1) where K_c is evaluated from (36) to be 212.7. The responses presented are for K=200. The LH traces clearly show marginal stability as expected from the linear analysis, (It is observed that control V_s slightly impinges the zero limit in transient which would be infeasible in practice of course). The RH traces show the response with the controller initiated slightly earlier i.e. from a larger initial deviation. This causes V_s to be driven above the value corresponding to S_{max} (eqn. 25) such that the process enters the negative gain region (of S versus V_s) with the result that it settles apparently at an incorrect steady-state as indicated. The steady-state values of S and V_s thus achieved are consistent with general steady-state formula (24).

3.2 Large Signal Closed Loop Behaviour

For gains K well below the critical value K_c, the linear proportional controller is stable and achieves the target steady state reference conditions S_{ref}, V_{sref} even from large initial deviations therefrom. The trace for K=100 (i.e. just less than 50% of K_c (=212.7) for case (a) shown in Fig. 14 is typical for such situations, even though the initial condition for the closed-loop test, i.e. S(0)=0.3333, is far removed from S_{ref} (=0.4563). The desired steady-state is also achieved, as again shown in Fig. 14, if the gain is raised to 148, although now there is a prolonged dwell in the response before it climbs to achieve the value of S_{ref}, following a small overshoot.

Increasing K slightly to 150 however causes another other feasible steady-state to be achieved (i.e. S=0.3637 and V_s=14.898) as a result of the V_s - transient exceeding the value given by eqn. (25) for S_{max}. The gain of 200, (which yields a stable response settling at $S=S_{ref}$ for small initial deviations : see Fig. 13) again produces an undesired solution for S=0.2359 and V_s=45.09, even further-removed from the desired separation of 0.4563.

The apparent steady-state nature of the higher gain solutions, e.g. for K=150 and 200 in Fig. 14 are somewhat difficult to explain. It is true that they are consistent with steady state equation (24) but the points achieved by the two responses (by τ=100 on Fig. 14) lie on the unstable i.e. negative gain portion of that steady-state characteristic. This fact prompted longer term experiments around in the gain region $148 \leq K \leq 150$ the results of which are shown in Figs. 15 and 16. Clearly the solutions at τ=100 in Fig. 14 for K=150 and 200, although of long duration, may be only temporary in the strict sense of the word. This claim is made since, as Fig. 15 and 16 show, as K in increased from 148.00 to 149.85, the dwell in the response becomes progressively longer, albeit a jump {to the (locally) stable steady sate of S=0.4563, V_s=1.0} ultimately occurs. For practical purposes, however, the excessively long dwell of τ=4000 compared to a low gain time constant of around τ=6.0 (see the response for K=100 in Fig. 14) is quite unacceptable. It is worth noting that other cases (e.g. case (d)) show similar trends.

4. Conclusions

The analytically-derived parametric models for the separation within CSTC distillation columns presented in ACSE RR573, 1995 have been comprehensively validated by numerical simulation and a wide range of typical results have been presented here. In particular, the equation for steady-state separation in terms of normalised column length L and volatility parameter α has been shown to make exact predictions for the operating condition $V_r = \alpha V_s$ ($L_s = \alpha V_r$). A more general separation formula in terms of vapour flow V_s specifically has been derived here and also validated. The non-linear characteristic relating S to V_s has been shown to exhibit a maximum turning point followed by a negative gain region, thus yielding two mathematical solutions for V_s for a given S. The transfer function models derived in RR573 have been shown here to yield transient step responses very similar to those obtained in simulation for small initial deviations from steady state and for small steps in V_s.

The above-mentioned non-linear steady-state characteristic explains why differences in large signal behaviour can be generated and in particular why large increases in V_s beyond the operating point $V_r = \alpha V_s$ can yield a steady-state reduction (rather than just the analytically predicted non-minimum-phase transient reduction) in separation. The physical explanation of the phenomenon is that, whereas a small increase in energy input (i.e. in V_s), will produce an increase in steady-state separation through increased evaporation, a large increase merely causes increased circulation and therefore increased physical mixing within the system overall, rather than increased thermodynamic separation.

Predicted local closed loop stability criteria have been verified over a wide range of plant and feed parameter space and interesting non-linear phenomenon also demonstrated. In particular, for proportional controller gains exceeding some 50% critical and for large initial deviations from the target steady state, an open-loop unstable solution on the above-mentioned negative-gain characteristic can be sustained for very long periods before switching to the desired solution. This is consistent with the many anecdotal reports of unpredictability of the separation control characteristic of columns. The models are here convincingly verified for self consistency and may safely be used in future theoretical control studies.

References

[1] Edwards, J. B and Mohd Noor, S B. : 'Interpretation and Utilisation of Parametric Models of Binary Distillation Columns : Relating Plant and Control Design', The University of Sheffield, ACSE Research Report No. 573, April 1995, 37pp.

[2] Banks, S. P and Mhana, K. J. : 'Optimal Control and Stabilisation for Non-linear Systems', IMA Journal of Mathematical Control and Information, 1992, Vol. 9, pp 179-196.

[3] Edwards, J. B and Mohd Noor S. B. : 'Use of the Riccati Equation On-line for Adaptively Controlling a CSTC Distillation Column', The University of Sheffield, ACSE Research Report No. 631, July 1996, in preparation.

[4] Edwards, J. B and Mohd Noor S. B. : ' Use of the Riccati Equation On-line for Adaptively Controlling a CSTR Chemical Reactor', The University of Sheffield, ACSE Research Report No. 576, Dec. 1995, 18pp.

[5] Rowlands, J. P. :' On-line Riccati Control of Chemical Reactors', The University of Sheffield, ACSE, Third Year Project Dissertation, June 1996, 70pp.

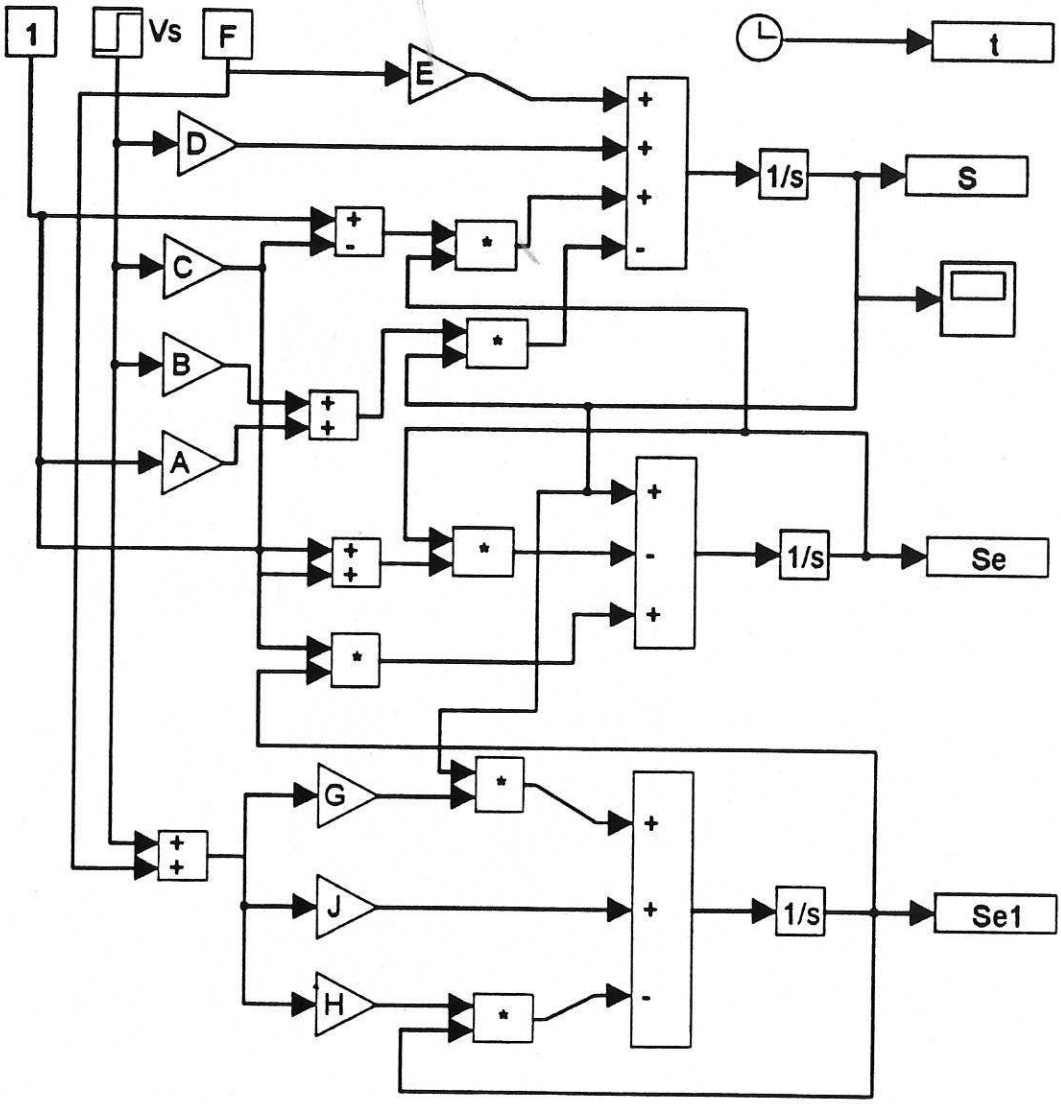

Fig. 1 SIMULINK block diagram for open loop process

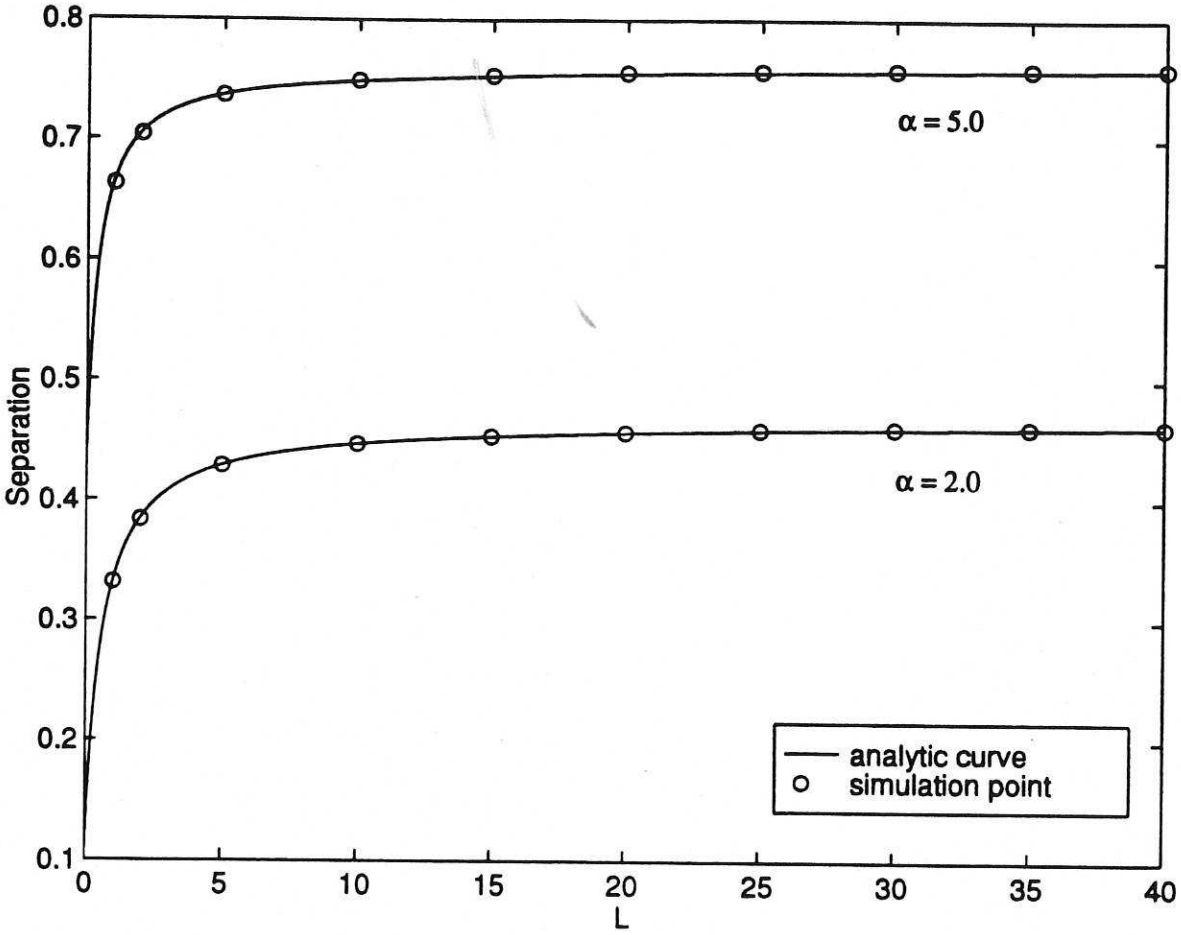

Fig. 2 Comparing quiescent steady-sate separations predicted analytically and by simulation

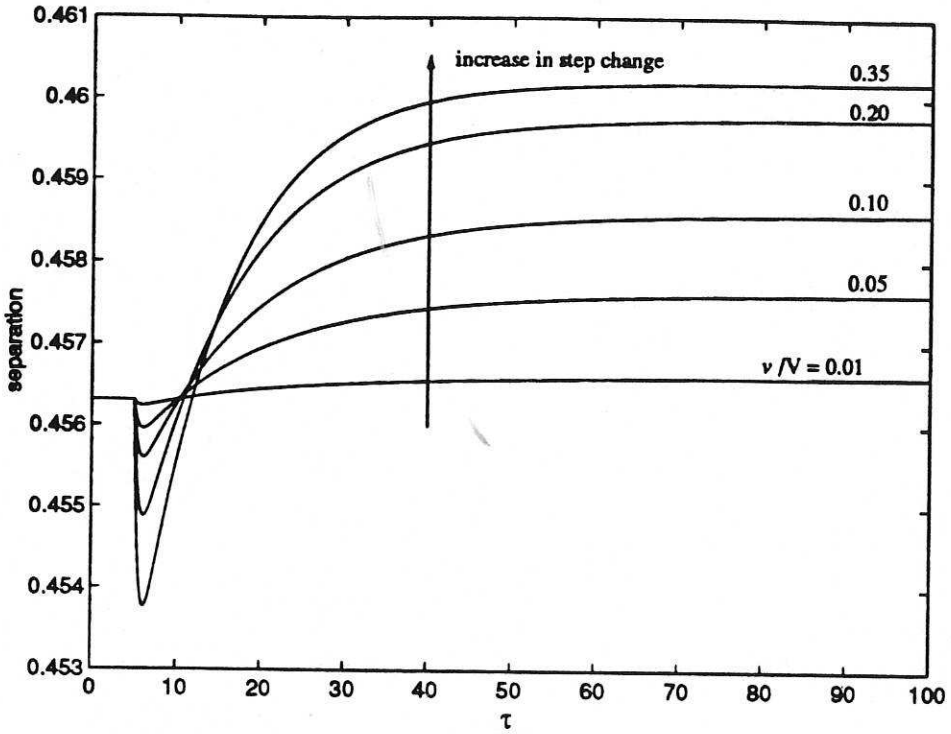

Fig. 3 Responses of separation, S to different step sizes, ν : Case (a)

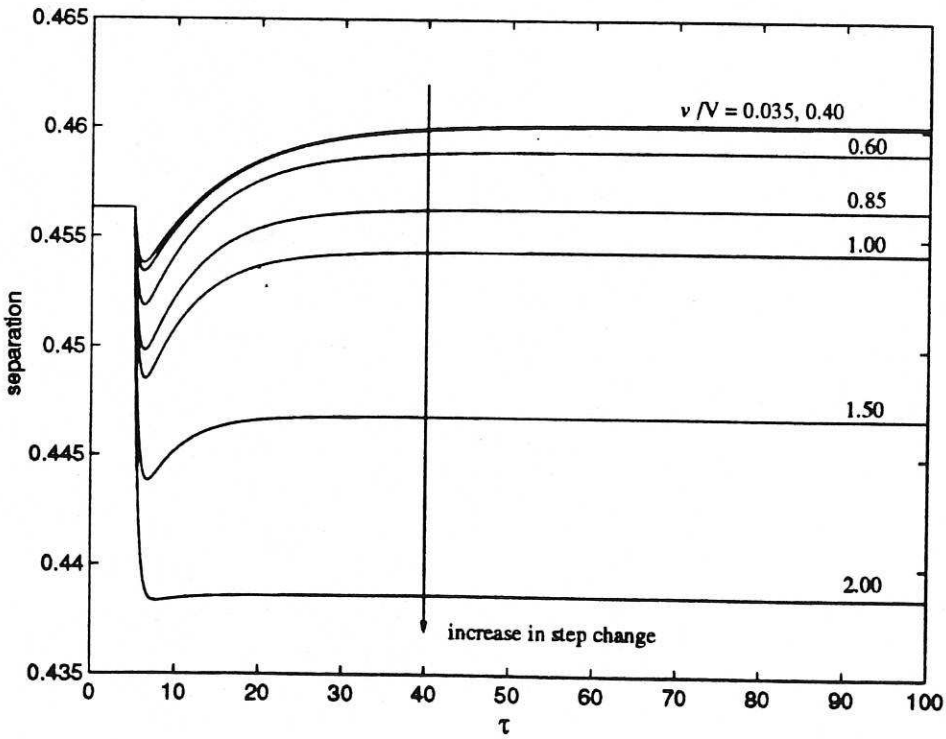

Fig. 4 Responses of S to large steps in ν : Case (a)

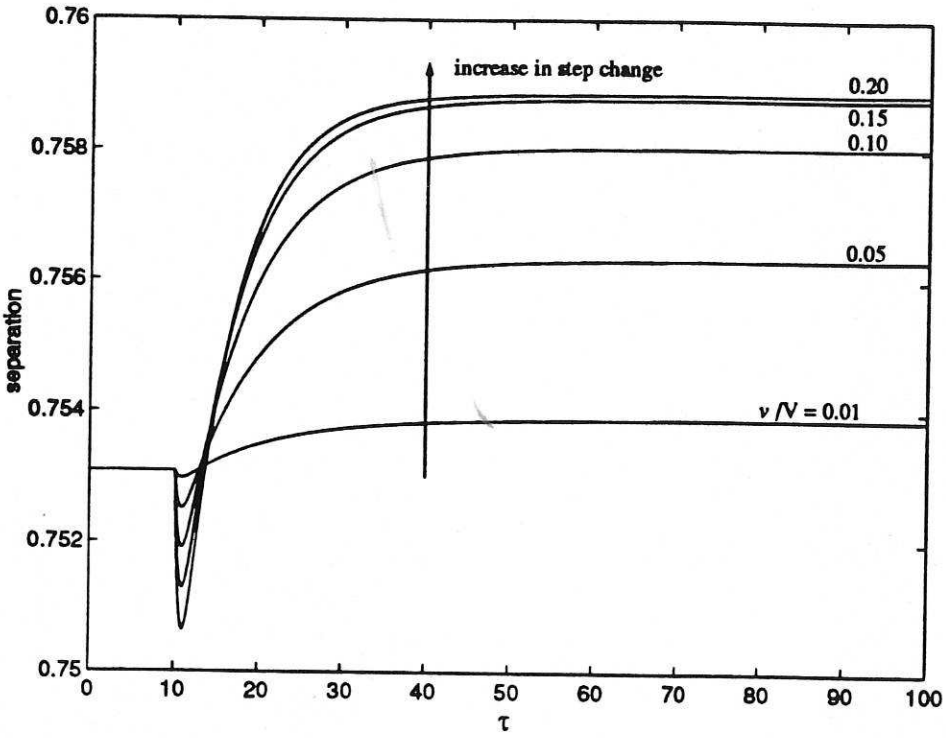

Fig. 5 Responses of separation, S to different step sizes, ν : Case (d)

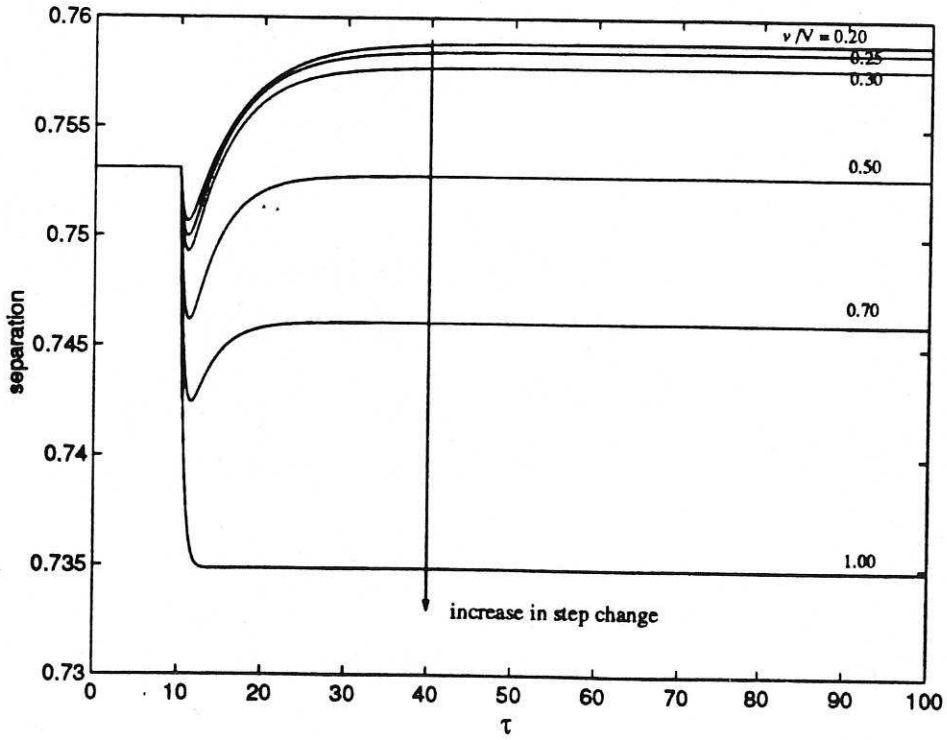

Fig. 6 Responses of S to large steps in ν : Case (d)

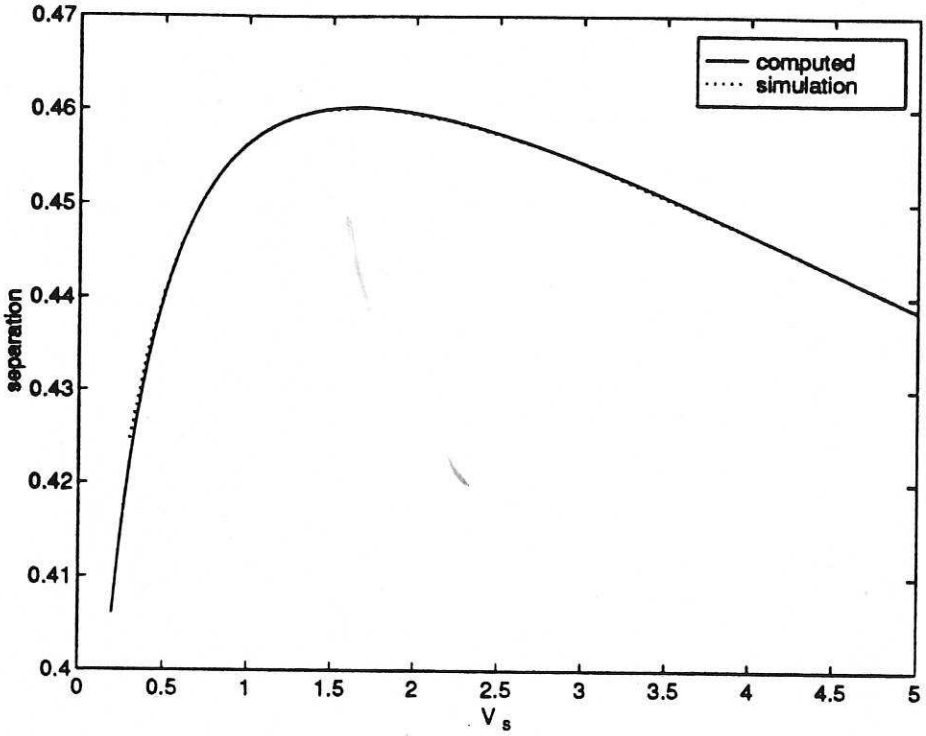

Fig. 7 Steady-state characteristic S versus V_s for case (a) : Analytically derived and by simulation

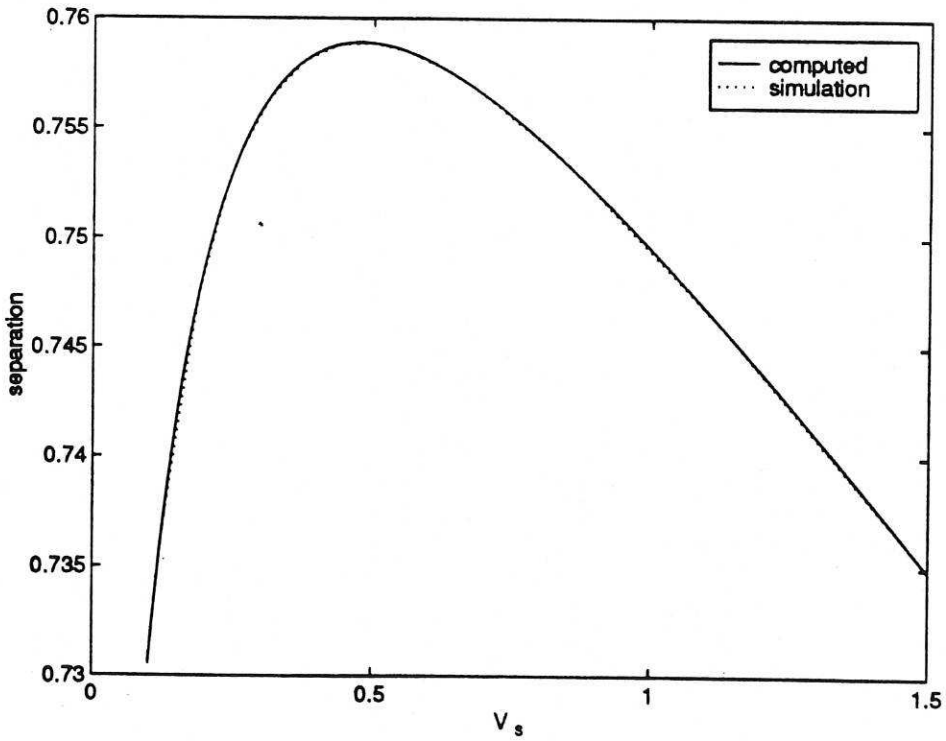

Fig. 8 Steady-state characteristic S versus V_s for case (d) : Analytically derived and by simulation

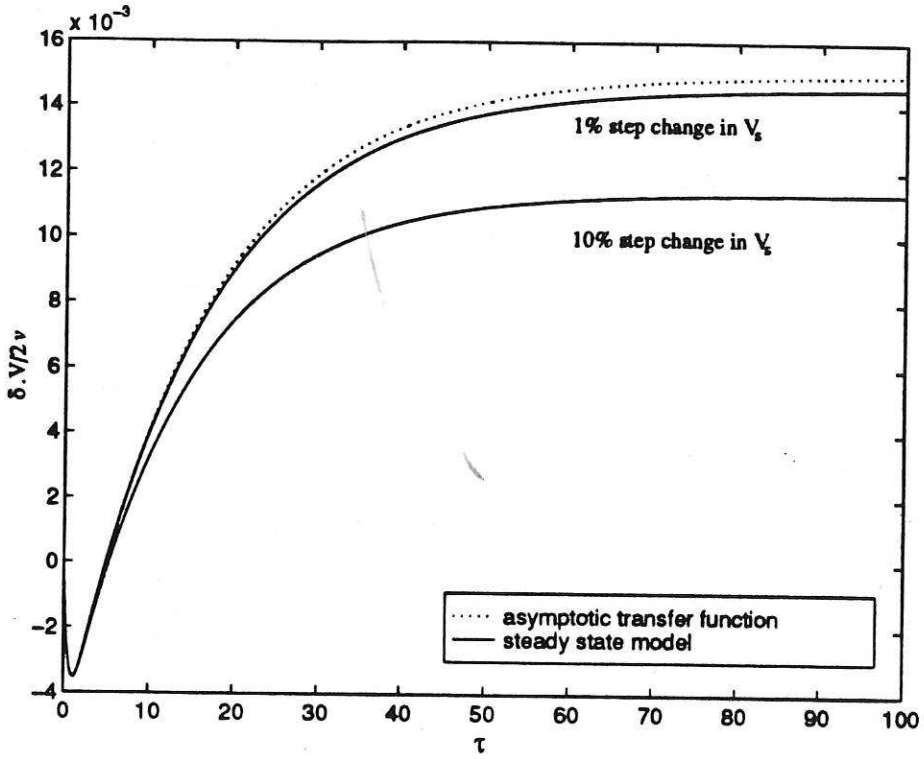

Fig. 9 (A) Comparing the simulated open-loop, unit step responses of the non-linear process for steps of $2v/V = 1.0\%$ and 10.0% with that of the linear asymptotic model. Case (a).

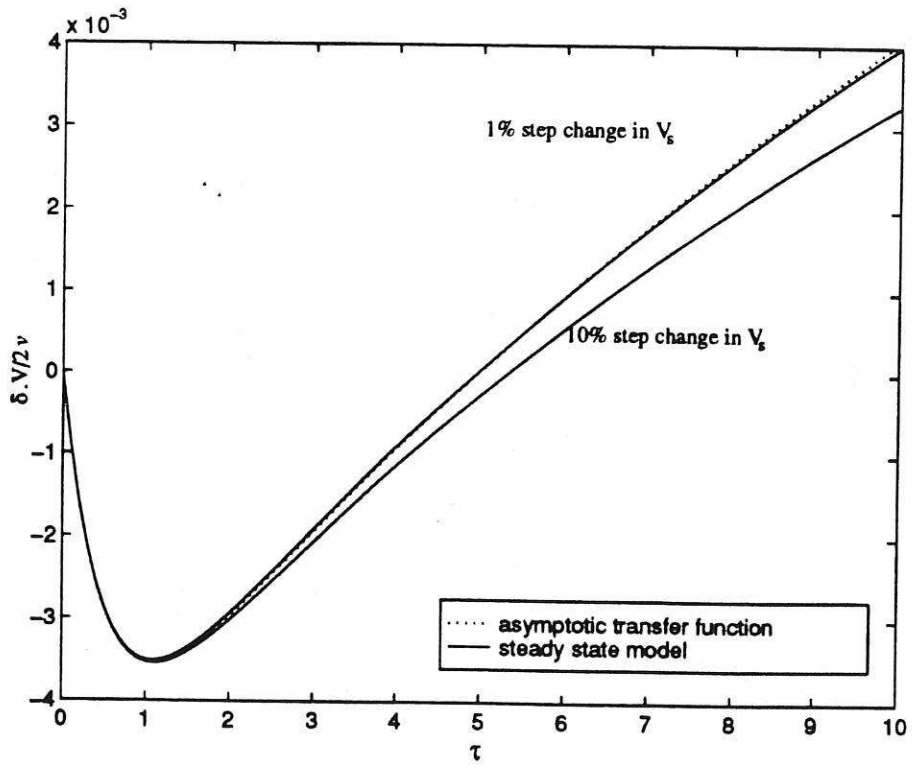

Fig. 9 (B) Zoomed display of initial responses of Fig. 9 (A)

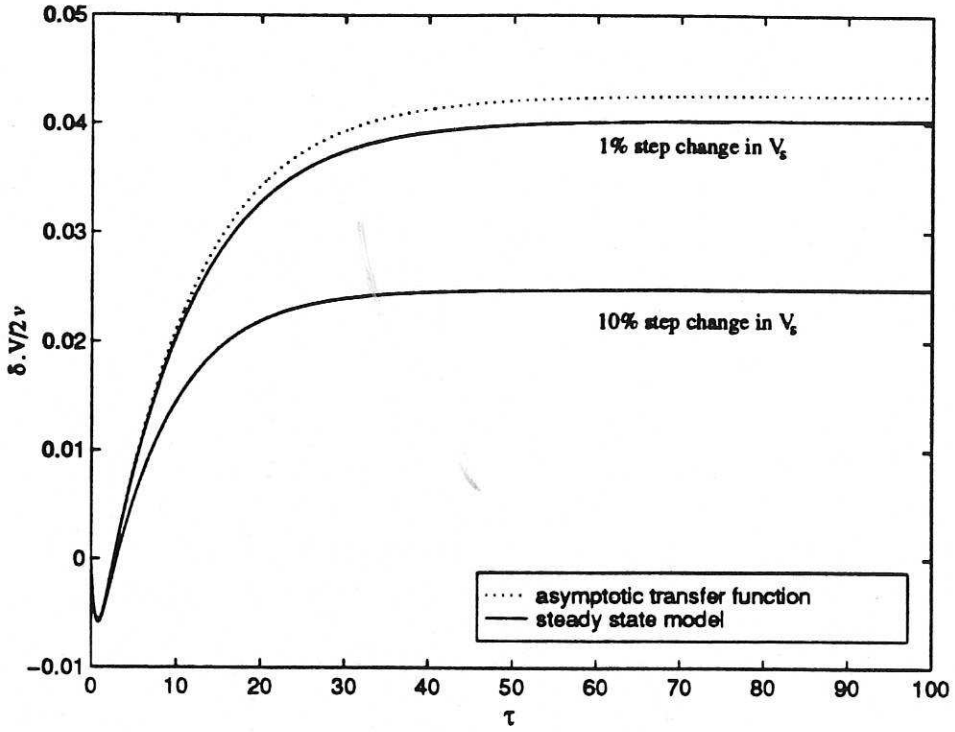

Fig. 10 (A) Comparing the simulated open-loop, unit step-responses of the non-linear process for steps $2\nu/V = 1.0$ % and 10.0% with that of the linear asymptotic model. Case (d).

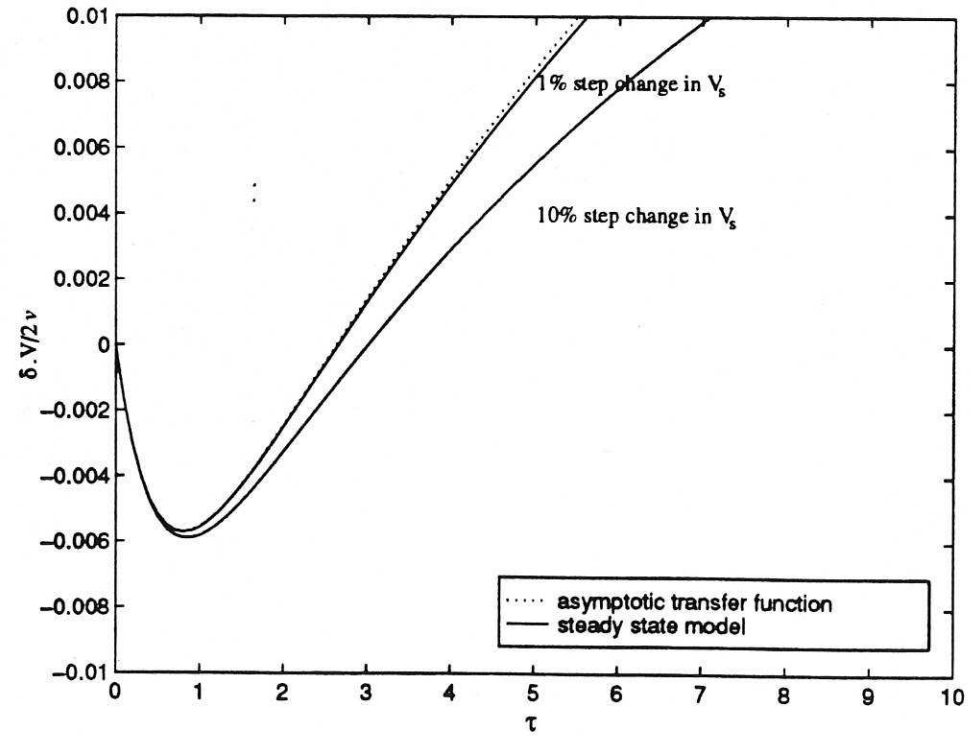

Fig. 10 (B) Zoomed display of initial responses of Fig. 10 (A)

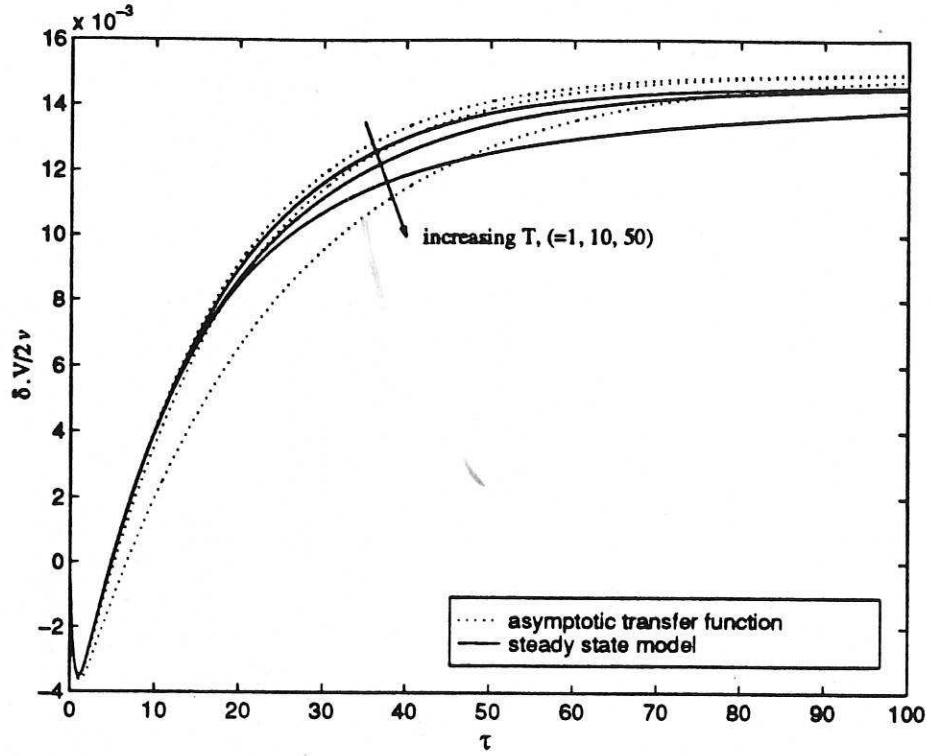

Fig. 11 (A) Showing the effect of increasing end vessel time constant on the unit step response. Case (a).

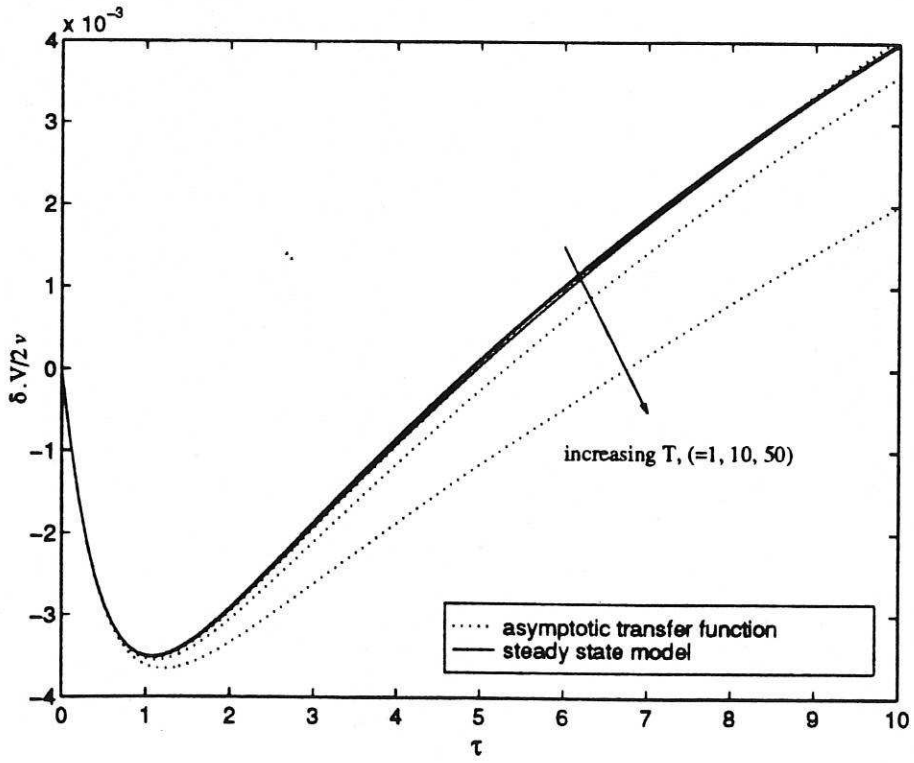

Fig. 11 (B) Zoomed display of initial responses of Fig. 11 (A)

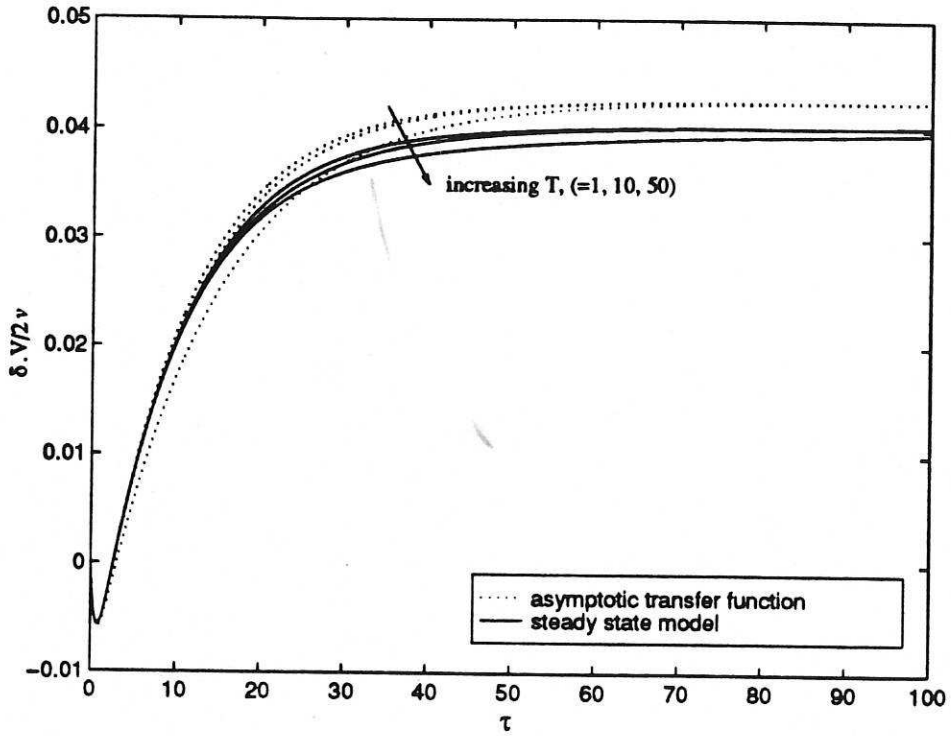

Fig. 12(A) Showing the effect of increasing end vessel time constant on the unit step response. Case (d).

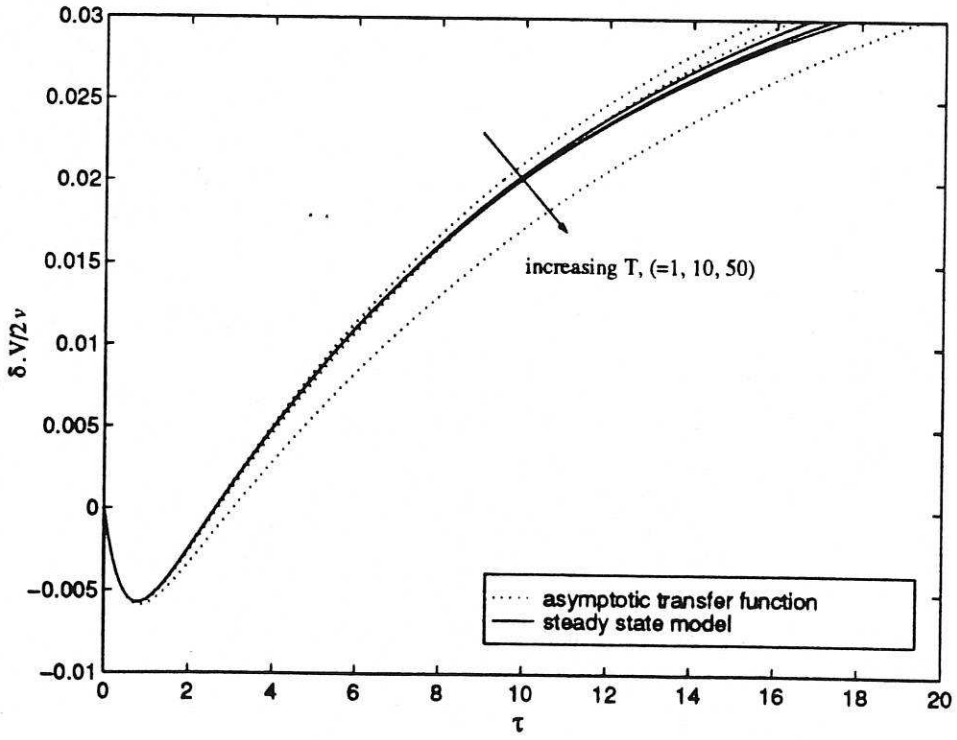

Fig. 12 (B) Zoomed display of initial responses of Fig. 12 (A)

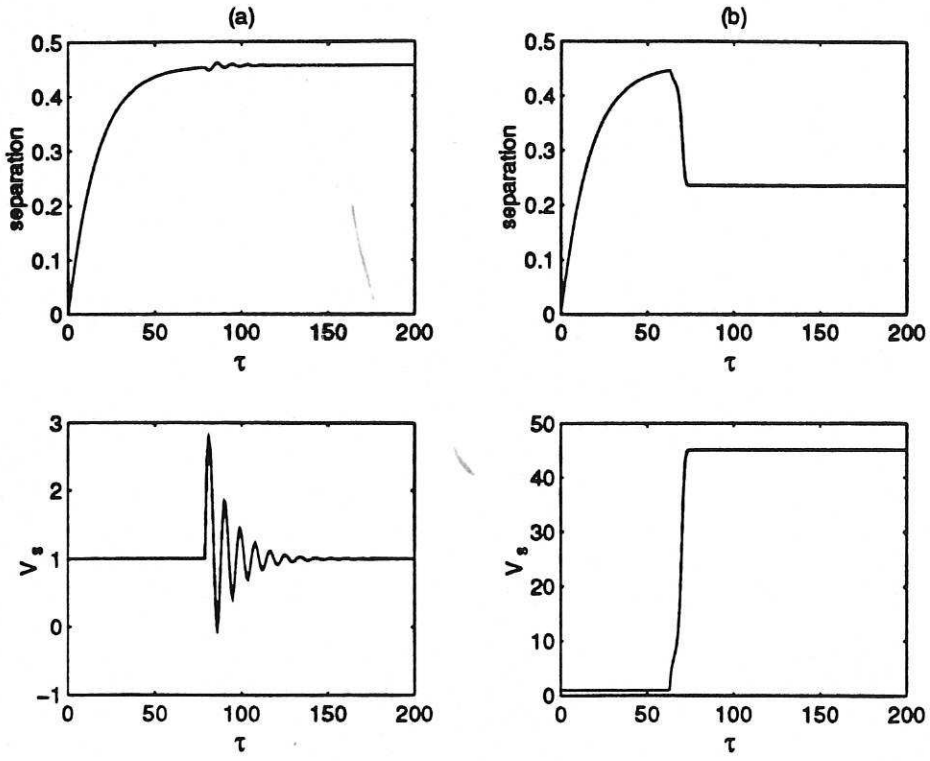

Fig. 13 Showing the effect of closing the control loop with a gain marginally less than the predicted critical value. Case (a), K=200.

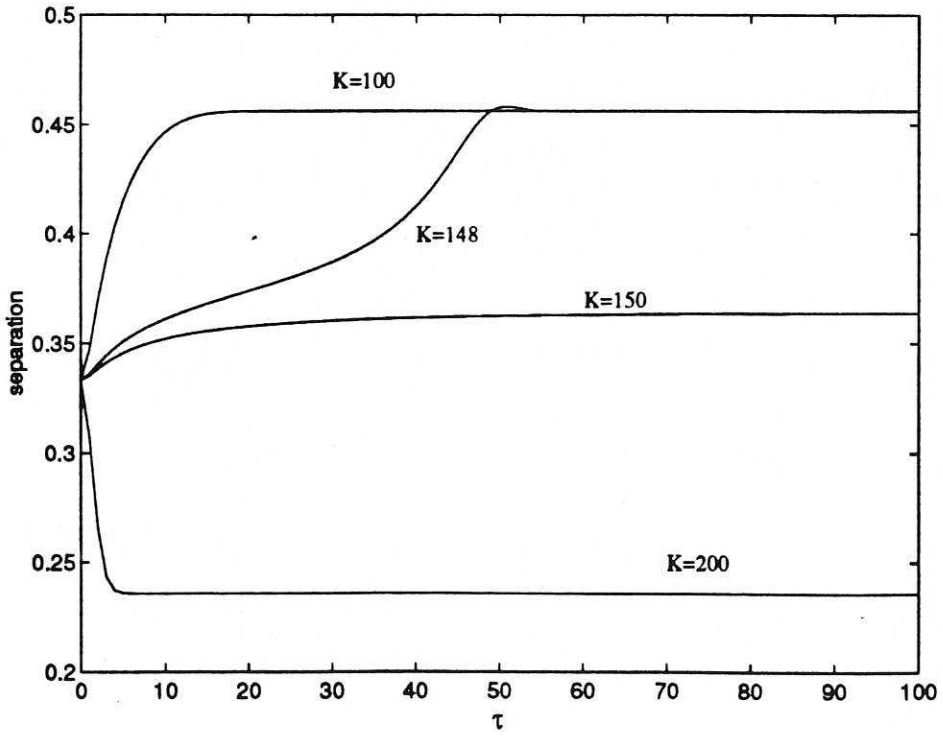

Fig. 14 Large signal behaviour under linear proportional closed-loop control. Case (a).

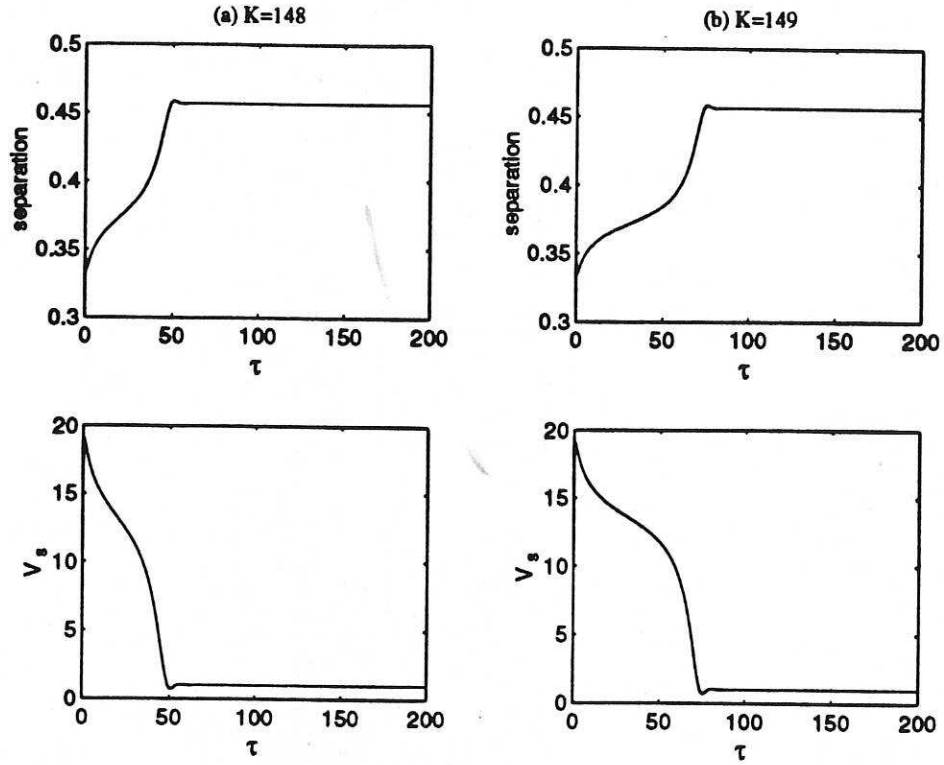

Fig. 15 Showing progressively long dwell in response for values of gain ≥ 148.

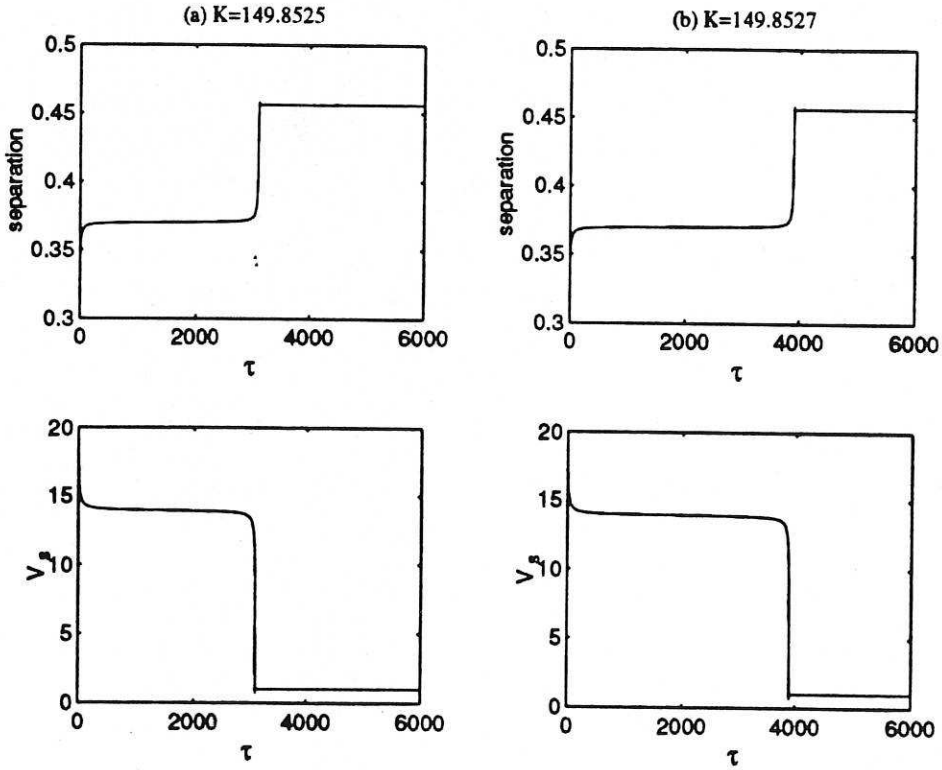

Fig. 16 Showing further increase of dwell time with only marginal increase in gain towards 150.

Appendix 1

Derivation of Steady-State Separation as a General Function of Vapour Rate, Under Constant-Feed and Symmetrical Operating Conditions.

From the steady-state version of process differential equations (11) and (12) we obtain :

$$\frac{(V_s+F)S+\alpha V_s S_e - F\varepsilon/(\alpha+1)-\varepsilon V_s}{kL'} = S_e - S = \frac{\alpha V_s\{S_e(1)-S_e\}}{kL'} \qquad (A.1)$$

and $$(V_s + F)\,(S - \alpha\, S_e(1) + \varepsilon\,) = 0$$

so that $$S_e(1) = (S + \varepsilon)/\alpha \qquad (A.2)$$

for $Vs + F \neq 0$.

Thus, we may eliminate $S_e(1)$ from the RHS of eqn. (A.1), using eqn. (A.2) to give :

$$S_e = \frac{S(1+V_s/kL')+\varepsilon V_s/kL'}{(1+\alpha V_s/kL')}$$

or $$S_e(kL'+\alpha V_s) = S(kL'+V_s)+\varepsilon V_s \qquad (A.3)$$

From the LHS of eqn. (A.1) we also obtain :

$$S_e(kL'-\alpha V_s) = S(kL'+V_s+F)-\varepsilon\{V_s(\alpha+1)+F\}/(\alpha+1) \qquad (A.4)$$

Eliminating S_e between equations (A.3) and (A.4) therefore yields

$$S = \left(\frac{\varepsilon}{\alpha+1}\right)\left[\frac{kL'\{2V_s(\alpha+1)+F\}+\alpha V_s F}{kL'(2\alpha V_s+F)+F\alpha V_s+2\alpha V_s^2}\right] \qquad (A.5)$$

This result is restated as eqn.(24) in the main text.

Calculation of Turning Point in S versus Vs Characteristic

It is convenient to write eqn. A.5 in the form

$$S = \frac{\varepsilon}{(\alpha+1)}\left[\frac{f(V_s)+aV_s}{f(V_s)+bV_s^2}\right] \qquad (A.6)$$

where $F(V_s) = cV_s + d$ so that $\partial f / \partial V_s = c$

and where $a = 2kL'$

$b = 2\alpha$

$c = \alpha(F+2kL')$

and $d = FkL'$

Thus, for the turning points in the curve of S versus V_s, $\frac{\partial S}{\partial V_s} = 0$ so that if $\dot{f}$ denotes $\frac{\partial f}{\partial V_s}$, we deduce that

$$\left(f+bV_s^2\right)\left(\dot{f}+a\right) - \left(f+aV_s\right)\left(\dot{f}+2bV_s\right) = 0 \qquad (A.7)$$

giving $$V_s^2\, b(c+a) + 2bdV_s - ad = 0 \qquad (A.8)$$

Solving quadratic eqn. (A.8) thus yields the values of V_s for the turning points in the S versus V_s characteristic, viz :

$$V_s = \frac{\pm\sqrt{db\,\{db+a(c+a)\}} - bd}{(c+a)b} \qquad (A.9)$$

and on substituting for a, b, c and d in terms of k, L', α and F, we deduce that, for the maximum value S_{max} of S

$$V_s\Big|_{S=S_{max}} = \frac{kL'}{\alpha\{\alpha F+2kL'(\alpha+1)\}}\left[\sqrt{2\alpha F\{\alpha F+kL'(\alpha+1)\}} - \alpha F\right] \qquad (A.10)$$

This result is presented as eqn. (25) in the main text.